Check for updates

JGR Space Physics

RESEARCH ARTICLE
10.1029/2021JA029379

Conditions for Topside Ion Line Enhancements

Theresa Rexer[1], Thomas Leyser[2], Björn Gustavsson[1], and Michael Rietveld[3]

[1]Institute for Physics and Technology, Arctic University of Norway UiT, Tromsø, Norway, [2]Swedish Institute of Space Physics, Uppsala, Sweden, [3]EISCAT Scientific Association, Ramfjordmoen, Norway

Key Points:

- Observations of high frequency enhanced ion line spectra at the topside ionosphere
- The appearance of the topside enhancements are affected by the proximity to the topside double resonance frequency
- We interpret the observations as a result of *L* mode wave propagation through artificial radio windows

Correspondence to:
T. Rexer,
theresa.rexer@uit.no

Citation:
Rexer, T., Leyser, T., Gustavsson, B., & Rietveld, M. (2021). Conditions for topside ion line enhancements. *Journal of Geophysical Research: Space Physics*, *126*, e2021JA029379. https://doi.org/10.1029/2021JA029379

Received 25 MAR 2021
Accepted 10 JUN 2021

Abstract Enhanced ion line spectra as a response to magnetic field-aligned high frequency (HF) pumping of the overdense polar ionosphere with left-handed circular polarization, can be observed at the top and bottomside F-region ionosphere under certain conditions. The European Incoherent Scatter (EISCAT) UHF radar was directed in magnetic zenith on October 18th and 19th, 2017 while stepping the pump frequency of the EISCAT Heating facility both upward and downward across the double resonance frequency of the fourth harmonic of the electron gyrofrequency and the local upper hybrid frequency, in a 2-min-on, 5-min-30-s-off pump cycle. We present observations of two separate cases of topside HF-enhanced ion lines (THFIL). THFIL simultaneous to bottomside HFIL (BHFIL), and conditioned by the relative proximity of the HF pump frequency to the bottomside double resonance frequency, consistent with previous observations (Rexer et al., 2018, https://doi.org/10.1029/2018JA025822) were observed for HF pulses on 19th October. Recurring THFIL appearing after BHFIL have faded and conditioned by the relative proximity to the double resonance frequency on the topside ionosphere, were observed on 18th October. The THFIL are consistent with transionospheric propagation through artificial radio windows by *L* mode guiding of the pump wave, facilitated by large scale density ducts present in the plasma.

1. Introduction

High power radio waves transmitted from the ground into the high-latitude ionosphere at frequencies below the critical frequency, are reflected, at altitudes depending on the plasma density and the polarization of the incident wave. Vertically propagating waves with an *O* mode polarization will reflect at the altitude where the pump frequency, f_{HF} is equal to the local plasma frequency, f_P. Pump waves in a horizontally stratified ionosphere transmitted at the Spitze angle, defined by $\sin(\theta_c) = \sin(\alpha)\sqrt{\frac{Y}{1+Y}}$, where $Y = \frac{f_{HF}}{f_G}$ and α is the angle of the magnetic field, in the magnetic meridian plane, from vertical (Budden, 1980), can pass through the radio window and continue to propagate to regions of higher plasma density and frequency (Mjølhus, 1990). Here f_G is the electron gyro frequency. Pump waves transmitted at larger angles to the vertical than the Spitze angle are reflected at progressively lower altitudes.

In this paper, we present observations of high frequency (HF) enhanced ion line spectra from the top and bottomside ionosphere during magnetic field-aligned, high-power pumping of the polar ionosphere. Ellis (1956) first observed ionogram signatures of pump wave propagation to altitudes beyond the *O* mode reflection height. Subsequently Ganguly and Gordon (1983) and Isham et al. (1990) presented incoherent scatter radar (ISR) measurements of HF modification experiments, showing effects of an HF pump wave above the *O* mode reflection altitude, at mid- and high-latitudes, respectively. Several studies have since reported ISR measurements showing effects of HF pumping above the reflection altitude of the ionospheric *F*-region (Isham, Hagfors, et al., 1999; Isham, Rietveld, et al., 1999; Kosch et al., 2011; Rietveld et al., 2002). Leyser et al. (2018) present signatures of transionospheric HF pump wave propagation into space in CASSIOPE spacecraft data. The first consistently recurring topside HF enhanced ion line (THFIL) spectra and their relation to pump frequencies close to the fourth gyroharmonic frequency were shown by Rexer et al. (2018). Observations of THFIL from an experiment in 2013 were also reported by Borisova et al. (2020).

An *O* mode wave, that is propagating strictly in a field-aligned direction is a left-hand circular polarized (LHCP) wave for which the electric field rotates opposite to the electron gyro motion, known as an *L* mode wave (i.e., Chen, 1983). The *L* mode dispersion curve follows the edge of the O mode dispersion surface where k is parallel to B for $f_{\mathrm{HF}} > f_P$ and the slow *X* mode band dispersion surface for $f_P > f_{\mathrm{HF}}$ (see for example

© 2021. The Authors.
This is an open access article under the terms of the Creative Commons Attribution-NonCommercial-NoDerivs License, which permits use and distribution in any medium, provided the original work is properly cited, the use is non-commercial and no modifications or adaptations are made.

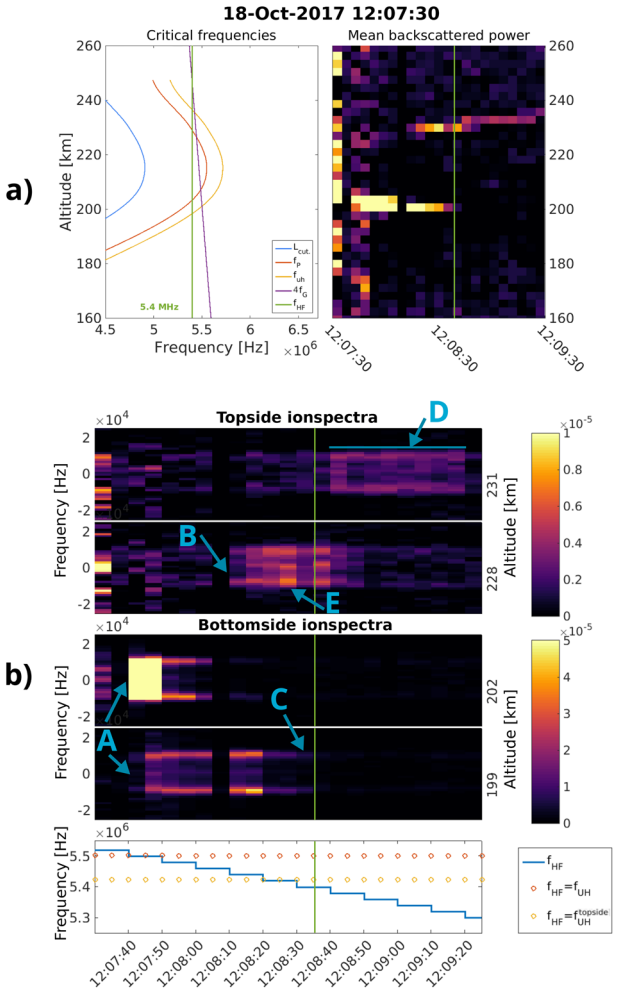

Figure 1. Example of a typical observation of case A topside high frequency enhanced ion lines (THFIL). (a) The top left panel shows the critical frequencies calculated from the observed natural Langmuir waves. The blue, red and yellow lines indicate the *L* mode cutoff, the local plasma frequency, and the local upper hybrid frequency, respectively. The purple line shows the fourth harmonic of the electron gyrofrequency, while the green vertical line indicates the frequency of the transmitted *O* mode pump wave. On the right the 5-s mean backscattered ion line power, with a 3 km altitude resolution, during a 2-min-on pulse is shown. The vertical green line in the top right panel plot indicates the time to which the left panel plot corresponds. (b) The four upper panels show the topside ion line spectra and the bottomside ion line spectra with the frequency on the vertical axis, for the two altitudes of the strongest THFIL (228 and 231 km) and bottomside high frequency enhanced ion lines (199 and 202 km). The bottom panel shows f_{HF} and the top- and bottom-side fourth harmonic of the double resonance frequency, corresponding to the panels above. Green vertical lines indicate the time corresponding to the top left panel in (a) of the critical frequencies.

Figure 1 in Nordblad & Leyser, 2010). The *X* mode branch of the *L* mode is sometimes called the *Z* mode (Mjølhus, 1990). However, this usually refers to all wave vectors at angles between the parallel and perpendicular to the ambient magnetic field, whereas the *L* mode only refers to wave vectors parallel and anti-parallel to the magnetic field. When mapped out for all angles of k to B, the two wave modes form two dispersion surfaces that connect at the Spitze angle when $f_P = f_{\mathrm{HF}}$ forming a radio window (Mjølhus, 1990). A strictly field-aligned incident wave in the *L* mode moves from one to the other dispersion surface at this point without a change in polarization. At the EISCAT facility in Tromsø, Norway, the Spitze angle, is around $\theta_c = 5°–6°$ south of zenith. An incident wave that passes through a radio window in the *L* mode will continue to propagate to higher altitudes and regions of higher plasma density and frequency until it encounters its cutoff at $f_{L-cut} = -\frac{f_G}{2} + \frac{1}{2}\sqrt{f_G^2 + 4f_P^2}$ (Leyser et al., 2018; Mjølhus & Flå, 1984).

For an *O* mode wave transmitted in magnetic zenith in the high-latitude ionosphere, propagating beyond the plasma resonance height, outside the natural radio window is possible by two mechanisms. New radio windows in the form of large scale density ducts, generated by small scale density striations existing naturally (A. V. Gurevich et al., 1995) or created by the pump wave (i.e., Eliasson & Leyser, 2015; A. Gurevich et al., 1998; Istomin & Leyser, 2001), can guide the incident *O* mode wave into the *L* mode at locations outside the standard radio window (Leyser & Nordblad, 2009; Nordblad & Leyser, 2010). Alternatively, resonant scatter on small-scale field-aligned density irregularities can transform an incident *O* mode pump wave to a *Z* mode wave in the region above the upper hybrid resonance layer, where $f_{UH}^2 = f_G^2 + f_P^2$, close to the bottomside reflection altitude (Mishin et al., 2001). While *L* mode propagation through artificial radio windows (Nordblad & Leyser, 2010) is possible through large scale density ducts, the *Z* mode scattering process (Mishin et al., 2001) is facilitated by small scale density striations. Meter-scale density striations are generated within seconds, while kilometer-scale density ducts form in timescales on the order of minutes (Basu et al., 1997). The formation of small-scale density striations also depends on f_{HF}, and for f_{HF} close to multiples of the electron gyro harmonic frequency the generation of striations is greatly reduced (Honary et al., 1999). A mechanism for generating THFIL for a vertically propagating O mode wave has been proposed by Eliasson (2008). They simulated a propagation process where an incident wave reaches the resonance altitude and efficiently converts to the *Z* mode, for low duty-cycle experiments (2%), minimizing the effect of density irregularities in an attempt to explain the observations by (Isham, Rietveld, et al., 1999). In the present experiments the duty-cycle was significantly higher (~26%) and the direction of propagation along the magnetic field. Hence it is unlikely to explain our current observations.

In the following paper we present ISR observations forming two separate cases of recurring THFIL during comparable ionospheric conditions and HF pump schemes, from experiments on October 18th and 19th, 2017 at the EISCAT facilities in Tromsø, Norway. Strong THFIL occurred repeatedly while stepping f_{HF} through the fourth harmonic of f_G and a possible, previously undetected, relation to the topside double resonance frequency of the local f_{UH} and $4f_G$ has been observed. Observations of the naturally existing Langmuir waves, made in the plasma line spectra of the EISCAT UHF radar, are used to calculate the electron density and critical frequencies during the experiments.

2. Experiment

On October 18th and 19th, 2017, during quiet geomagnetic daytime conditions, the EISCAT Heating facility (Rietveld et al., 2016) in Tromsø was transmitting a LHCP HF radio wave in the magnetic zenith direction (78° elevation south), in a 2 min on - 5 min 30 s off cycle. Upon reaching the ionosphere most of the wave energy is in the *O* mode.

Different frequency stepping schemes were used on the two days, aiming to meet the double resonance frequency f_{dbl} on the bottomside ionosphere at some point during each heating cycle. The double resonance frequency is defined as

$$f_{dbl} = f_{UH} = 4f_G$$

and can be met by f_{HF} twice, once at the topside and once at the bottomside ionosphere. In this experiment, f_{HF} was changed in steps of 10 kHz every 10 s within the 2 min HF pulse, such that it crossed f_{dbl} on the bottomside. Because f_{HF} is stepped throughout each HF pulse and f_G decreases with increasing altitude, the numeric value for f_{dbl} on the topside will be different from the numeric value of f_{dbl} on the bottomside. On October 18th, 2017 the effective radiated power (ERP) in the *O* mode was estimated to be 378 MW and the frequency stepping was done from a few tens of kilohertz above f_{dbl} to a few tens of kilohertz below f_{dbl} on the bottomside ionosphere. The mean difference between the maximum ionospheric plasma frequency and the pump frequency, $\bar{m} = f_{OF2} - f_{HF}$, had a minimum value of $\bar{m}_{min} = 152$ kHz during HF pulses, while the maximum was $\bar{m}_{max} = 396$ kHz. On October 19th, 2017 the ERP in the O mode was estimated to be 460 MW with one extra transmitter running. The frequency stepping, alternated between stepping up from below to above f_{dbl} and stepping down from above to below f_{dbl}. For pulses on the 19th October, $\bar{m}_{min} = 603$ kHz, while $\bar{m}_{max} = 810$ kHz.

The EISCAT UHF radar, pointing in the magnetic field aligned direction, was used to obtain the ionospheric plasma parameters for the background and HF-modulated conditions. Measurements were done with the beata modulation scheme (i.e., Tjulin, 2017), giving a frequency resolution of 2.4 kHz, range resolution of 3 km and a temporal resolution of 5 s for ion line measurements. In addition, the plasma line is sampled at 0.4 μs lag profiles, averaged over 5 s, covering a 3.125 MHz wide band offset from the transmit frequency by 8.4, 6.0, and 3.4 MHz, and covering ranges from 107 to 374 km. Backscatter from natural existing Langmuir waves is observed during the experiment in the downshifted plasma line spectra that is −6.0 MHz offset from the radar transmit frequency. The electron density used for the calculation of relevant resonance and cut-off frequencies (f_P, f_{UH}, $f_{L-\mathrm{cut}}$) is obtained from these observed natural Langmuir waves in the plasma line spectra and adapting the method described by Hagfors and Lehtinen (1981) (see Section 3 of Rexer et al., 2018, for a detailed description).

3. Experimental Results

Observations made during the experiments show characteristic differences with respect to the appearance of bottomside HF enhanced ion lines (BHFIL) and the proximity of f_{HF} to the top- and bottomside f_{dbl} on October 18th and 19th. We have identified two cases for excitation of THFIL. In the following two sections, these observations are presented separately

3.1. Case A: October 18th Observations

On October 18th 2017, 16 HF pulses with clear THFIL were observed. Figure 1 shows an example of one of these. In the left panel of Figure 1a, the altitude profiles of, f_P, f_{UH}, $4f_G$, and $f_{L-\mathrm{cut}}$ are shown, for an altitude range from 180 to 280 km, at the time of strong THFIL (indicated by the vertical green line in the right panel). The right panel shows the altitude profile from 180 to 280 km of the mean ion line spectra power for the 2 min HF pulse with a 5 s temporal resolution. The development of the BHFIL and THFIL for the duration of the HF pulse as f_{HF} is stepped downward, is seen at altitudes around 202 and 228 km respectively.

The development of the ion line spectra of the BHFIL and THFIL for the duration of the HF pulse are shown in more detail in Figure 1b. Ion line spectra at the two altitude ranges of the strongest THFIL (228 and 231 km) and BHFIL (199 and 202 km) are shown in the four upper panels, while the f_{HF} stepping

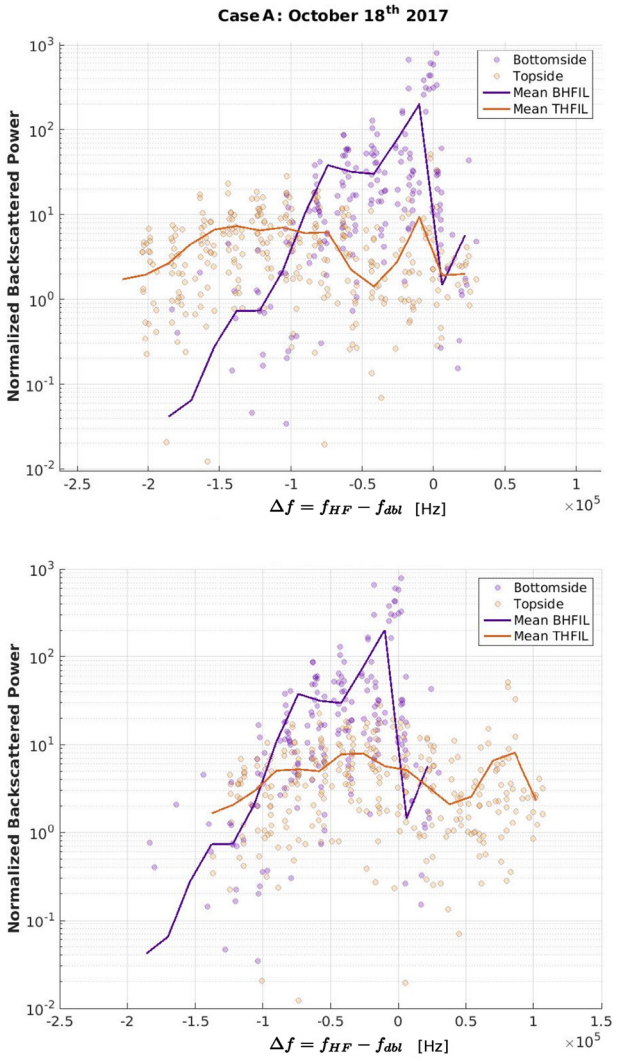

Figure 2. Comparison of all 16 high frequency pulses of case A. Normalized backscattered ion line power relative to the difference of the pump and bottomside double resonance frequency are shown upper panel. The lower panel shows the backscattered ion line power for the topside high frequency enhanced ion lines related to the topside double resonance frequency and the bottomside high enhanced ion lines related to the bottomside double resonance frequency. Topside enhancements are shown in orange while bottomside enhancements are shown in purple. The superposed solid lines show the mean of the observations.

scheme of 20 kHz decrements every 10 s is indicated in the bottom panel. The f_{dbl} at the bottomside (red) and topside (yellow) are also indicated. Green vertical lines indicate the time corresponding to the left panel in (a). In the first 5 s after Heating on, of the four upper panels in (b) (and the right panel in [a]), the commonly observed overshoot (Stubbe, 1996) is clearly visible. Five features are indicated in (b). (A) At 12:07:40 UT, as $f_{\mathrm{HF}} = 5.50$ MHz, after a first 20 kHz downward frequency step toward the bottomside f_{dbl}, the BHFIL appear strongly at 202 km and somewhat weaker at 199 km. (B) THFIL appear, faintly at first, around 228 km as $f_{\mathrm{HF}} = 5.44$ MHz, 50–60 kHz below $f_{dbl} \approx 5.5$ MHz at the bottomside. (C) BHFIL decrease in intensity and fade completely as $f_{HF} = 5.40$ MHz and lower. (D) The THFIL are visible for the remaining steps of f_{HF} of the HF pulse, increasing in altitude to 231 km (and 234 km as seen in the right panel of (a)) as f_{HF} is stepped further downward to 5.3 MHz. (E) The strongest THFIL were observed when $f_{\mathrm{HF}} = 5.42$ MHz at which only weak BHFIL were observed, during 3 steps ($f_{\mathrm{HF}} = 5.44$, 5.42 and 5.40 MHz) of simultaneous enhancements at both altitudes. BHFIL were observed at an altitude between the matching height (Rietveld et al., 2000) and the altitude where $f_P = f_{\mathrm{HF}}$. THFIL were observed at the reflection altitude.

We plot the backscattered power for all 16 HF pulses, with identified THFIL, observed on the October 18th, 2017, at the altitude of the strongest BHFIL and THFIL and relate this to the difference between f_{HF} and f_{dbl} on the bottomside and topside ionosphere, $\Delta f = f_{\mathrm{HF}} - f_{\mathrm{dbl}}$, in Figure 2. Solid lines indicate the mean of the observations of the backscattered ion line spectra power. In the upper panel we relate all observations of HFIL to f_{dbl} on the bottomside ionoshpere. The lower panel shows the same data where the BHFIL are related to the bottomside f_{dbl}, while the THFIL are shown relative to f_{dbl} on the topside ionosphere. The slight difference in the mean calculations (solid lines) of the two panels is due to the bining algorithm. THFIL occur primarily when f_{HF} is between 75 and 160 kHz below f_{dbl} on the bottomside, and the strongest THFIL occurred when no BHFIL were observed. In the lower panel we observe that the THFIL were strongest when f_{HF} was between 100 kHz below and 10 kHz above the f_{dbl} on the topside ionosphere. A narrow local maximum of the THFIL is also seen when f_{HF} is ≈ 70–90 kHz above f_{dbl} on the topside. From the upper panel it is apparent that these THFIL occurred when f_{HF} was at or just below the f_{dbl} on the bottomside. BHFIL also have a maximum here. Looking at the development of each HF pulse separately as illustrated for one pulse, in Figure 1, we see that the THFIL coincidental with the strongest BHFIL, are not part of the prolonged main THFIL visible from $\Delta f \approx -0.6$ to $\Delta f \approx -2.0$. These THFIL were visible as a "flare" of enhancement for ~5–10 s and faded thereafter, for some pulses (HF pulses starting at 10:07:30, 10:15:00, 11:00:00, 11:52:30, 12:00:00 and 12:07:30 UT), before disappearing and growing later during the HF pulse as f_{HF} was stepped downward.

In the example shown in Figure 1 the strongest THFIL is observed when f_{HF} is well below f_{dbl} on the bottomside. This is seen for all THFIL observed on October 18th and is also noticeable from the comparison of all pulses, in the top panel of Figure 2. Here we see that the solid orange line, indicating the mean backscattered power of all THFIL, has a wide local maximum well below f_{dbl} on the bottomside (zero on abscissa). Comparing the mean of the THFIL and BHFIL (orange and purple dots and lines) it is also clear that THFIL predominantly appeared when no BHFIL were observed and that, although the BHFIL were generally stronger than the THFIL, the strongest THFIL did not occur simultaneous to the strongest BHFIL. The narrow peak of the orange and purple solid lines in the top panel show that both BHFIL and THFIL

have a local maximum when f_{HF} is just below f_{dbl} on the bottomside. Figure 2 also shows that all THFIL have a comparable enhancement for comparable Δf, and that the enhancements develop and increase as Δf increases and the BHFIL begin to fade. The same data is shown in the lower panel of Figure 2 now arranged such that the THFIL (orange) are shown in relation to f_{dbl} on the topside, while the BHFIL (purple) are unchanged and shown in relation to f_{dbl} on the bottomside. The THFIL have a maximum when f_{HF} is just below f_{dbl} at the topside ionosphere.

The BHFIL in case A appear when f_{HF} is just below or at f_{dbl} in the bottomside ionosphere, in approximately the same range of Δf for f_{dbl} on the bottomside (Δf between ~−100 and ~6 kHz), as THFIL for Δf to f_{dbl} on the topside. Hence, as seen in the example in Figure 1, the strongest THFIL do not appear simultaneous to the strongest BHFIL (as in case B), but at f_{HF} where BHFIL have faded or disappeared completely. Consistent with the ion line spectra, the strongest enhancements, shown at two topside- and two bottomside altitudes in the middle panels of Figure 1, are observed at the resonance altitude, where $f_{HF} = f_P$, for the THFIL and between the matching height and the resonance altitude for BHFIL at the bottomside. At both the altitudes of THFIL and BHFIL, two well developed shoulders are seen, and we interpret these as decay lines of the parametric decay instability (PDI). These are more pronounced at the bottomside enhancements. A visible, but weak, central feature typical for the oscillating two stream instability (OTSI) (i.e., Kuo et al., 1997; Stubbe et al., 1992) is observed at the bottomside, while for the strongest THFIL the spectrum is filled in between the ion acoustic shoulders.

Downstepping HF pulses made on the October 19th, 2017, shown in the right column of Figure 3, are comparable to HF pulses where case A THFIL were observed. Although ion line spectra of the BHFIL (not shown) of these pulses are comparable to those of the case A observations as well as the range of the frequency steps in relation to f_{dbl} on the bottomside ionosphere, no THFIL were observed. The lower panels of Figure 3 indicate f_{dbl} on the top and bottomside ionosphere in relation to f_{HF}. Here we see that the range of frequency steps used in the downstepping experiment did not extend to or well below the topside f_{dbl}, the frequency range where we expect case A THFIL.

3.2. Case B: October 19th Observations

Figure 3 shows all HF pulses from 10.00.00 UT to 10.50.00 UT on 19th October in chronological order. Upper panels are the same as the upper right panel in Figure 1, showing the evolution of the mean ion line power at all altitudes, during a 2 min Heating on period with 5 s resolution. f_{HF} and the double resonance frequencies are indicated in the lower panels. As the direction of the frequency stepping in the experiment alternated between increasing and decreasing frequency for every Heating on pulse, the left column in the Figure shows all pulses where f_{HF} was stepped upward. It is only in these four pulses that we observe THFIL. During the HF pulses where f_{HF} was stepped downward, shown in the right column, only BHFIL are observed and no THFIL. In the top panel of the left column, showing the HF pulse starting at 10:06:00 UT, the THFIL appear weakly around 269 km for the initial 10 s frequency step. No THFIL are observed for the next 6 steps, until f_{HF} = 5.44 MHz and faint THFIL are observed for the two frequency steps just below and at the double resonance frequency. The second panel on the left shows slightly stronger THFIL around the same altitude for the fist frequency step. Weak THFIL are visible for three frequency steps of f_{HF} around the double resonance frequency, for f_{HF} = 5.44, 5.46 and 5.48 MHz. In the next two rows on the left column, showing HF pulses starting at 10:30.00 UT and 10:42:00 UT, THFIL are visible from Heating on and through all frequency steps until f_{HF} reaches the double resonance frequency around f_{dbl} = 5.48 MHz, where the THFIL fade.

Figure 4 is in the same format as Figure 1, but showing one of the four HF pulses of case B, in more detail. The backscattered power of BHFIL and THFIL increases as f_{HF} is increased stepwise and approaches the f_{dbl} on the bottomside ionosphere. The strongest THFIL are observed simultaneous to the strongest BHFIL at the altitude of the respective plasma resonance frequency, $f_P = f_{HF}$, rather than the matching height (Rietveld et al., 2000), which is ~7 km lower in altitude on the bottomside for the duration of the experiment on this day. While weaker than the BHFIL, the THFIL show a comparable development as the BHFIL, increasing in intensity while f_{HF} is stepped upward to the bottomside f_{dbl} and fading when $f_{HF} > f_{dbl}$. These case B observations are consistent with observations made in 2016 (Rexer et al., 2018).

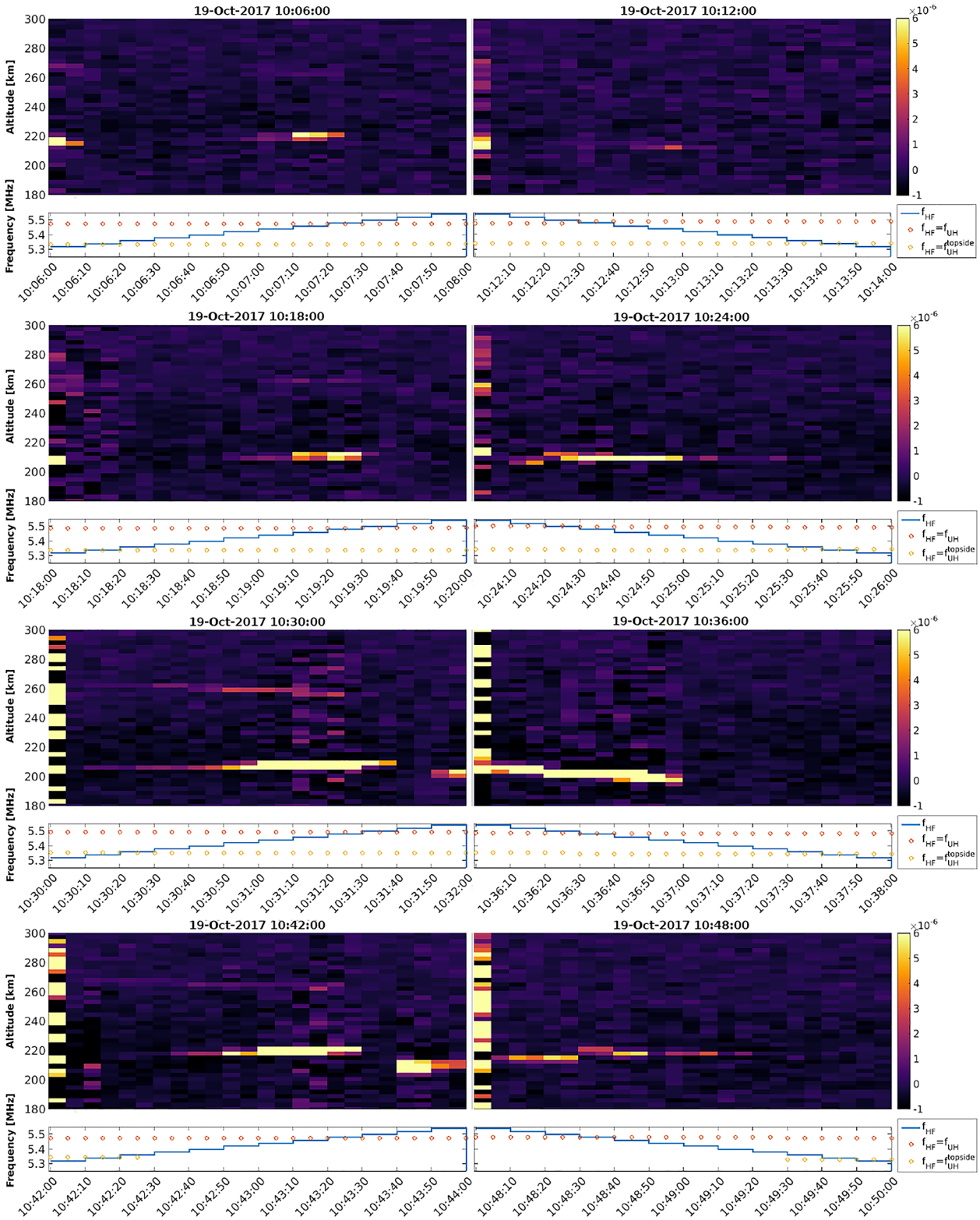

Figure 3. Case B: Time evolution of the averaged backscattered power in the ion line spectra for consecutive heating on pulses on October 19th, 2017. The bottom panels show f_{HF} and double resonance frequency. Case B enhancements are observed in high frequency pulses where f_{HF} is stepped upward (left column).

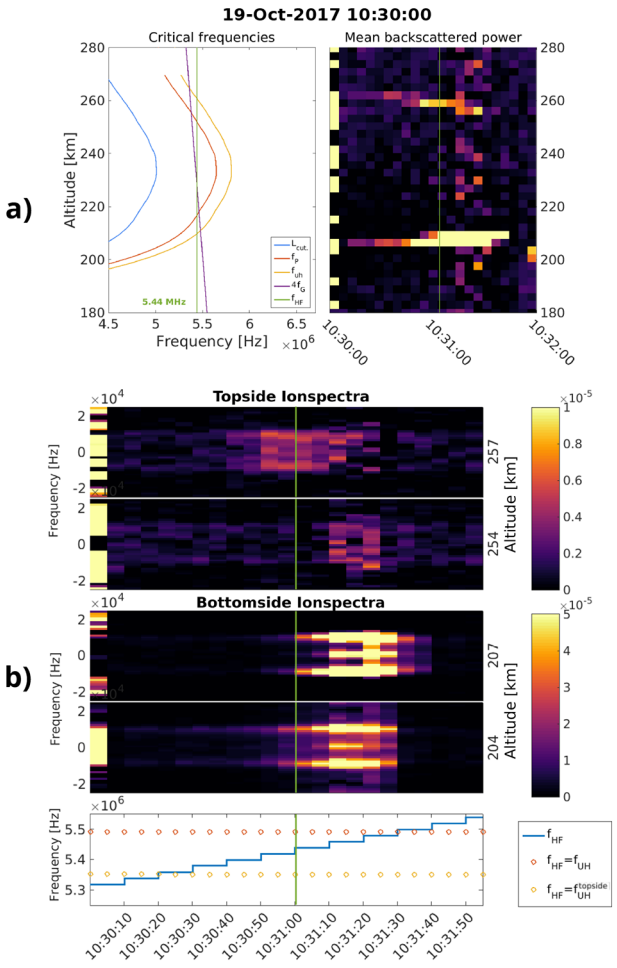

Figure 4. Example of a typical observations of case B. (a) The left panel shows the critical frequencies calculated from the observed natural Langmuir waves. The blue, red and yellow lines indicate the *L* mode cutoff, the local plasma frequency, and the local upper hybrid frequency, respectively. The purple line shows the fourth harmonic of the electron gyrofrequency, while the green vertical line indicates the frequency of the transmitted *O* mode pump wave. On the right the 5 s mean backscattered ion line power, with a 3 km altitude resolution, during a 2 min HF on pulse is shown. The vertical green line in the top right panel plot indicates the time to which the left panel plot corresponds. (b) The four upper panels show the topside ion line spectra and the bottomside ion line spectra with the frequency on the vertical axis, for the two altitudes of the strongest topside high frequency ion lines (254 and 257 km) and BHFIL (204 and 207 km). The bottom panel shows f_{HF} and the top- and bottomside fourth harmonic of the double resonance frequency. Green vertical lines indicate the time corresponding to the left panel of (a).

Figure 5 is the same as Figure 2, but for the case B data, with the 4 case B HF pulses from October 19th, 2017. Additionally, 33 HF pulses with THFIL, previously presented by Rexer et al. (2018), and all consistent with and categorized as case B, are added. We include the data again here to emphasize the case B characteristics and differences to case A. Case B has been previously discussed and the findings include observations that the case B THFIL are conditioned by the proximity of f_{HF} to f_{dbl} on the bottomside ionosphere. Additionally the THFIL only appear simultaneous to BFHIL and are generally weaker (Rexer et al., 2018). This is seen in the top panel of Figure 5. Relating the backscattered power of the THFIL to the topside f_{dbl}, shown in the lower panel, a small local maximum of the mean backscattered power of the THFIL can be observed when f_{HF} is close to f_{dbl} on the topside (zero on abscissa).

We have summarized the main characteristic of the BHFIL and THFIL for the two cases in Table 1.

4. Transionospheric Wave Propagation

Mjølhus and Flå (1984) adapted the theory of linear conversion of incident radiowaves into electrostatic waves, to ionospheric modification experiments, finding that an O mode wave transmitted into the horizontally stratified ionosphere can access the plasma resonance region through the radio window. That is, if $f_{\mathrm{HF}} > f_{L-\mathrm{cut}}$ the wave will propagate to the topside resonance region of the ionosphere, and continue through the topside radio window into space. Rays near θ_c are partially reflected and partially transmitted. Thus, partially penetrating rays at the bottomside radio window, will propagate to the topside ionosphere at an angle slightly off θ_c. These rays will be partially reflected at the topside radio window into a northward path (Mjølhus, 1990; Mjølhus & Flå, 1984).

Additionally, artificial radio windows can be generated at different locations by large scale, field aligned, density ducts induced by the pump wave (Leyser & Nordblad, 2009; Nordblad & Leyser, 2010). An incident O mode wave can be guided into the *L* mode along the geomagnetic field by ducts, with the same polarization as a ray at the critical angle in a horizontally stratified ionosphere. At $f_{\mathrm{HF}} = f_P$, with k exactly along the magnetic field, the O, *Z* and Langmuir dispersion surfaces connect, forming a radio window such that O mode waves guided into the *L* mode by large scale density irregularities will not change polarization. A wave, thus guided can pass the ionospheric density peak if $f > f_{L-\mathrm{cut}}$, and propagate to the topside resonance region, at different locations depending on the location and local parameters of the guiding density striation.

The dispersion properties of the upper hybrid waves is such that formation of small scale density striations, that can form a larger scale duct, decreases as the pump wave frequency approaches that of the double resonance frequency (i.e., Mjølhus, 1993; Robinson et al., 1996). Anomalous absorption is also at a minimum near or at harmonics of f_G (Stubbe et al., 1994). Consequently, and consistent with previous observations (Honary et al., 1999), coupling to Langmuir waves and ion acoustic waves is possible. Contrary to small scale density striations, large scale density ducts generated by the pump wave (i.e., A. Gurevich et al., 1998; Kelley et al., 1995) have a longer generation and decay time, on the order of minutes (Basu et al., 1997). Thus, guiding of the pump wave into the *L* mode, and hence transionospheric propagation, can be facilitated by these as they may exist in the plasma for several minutes, also when f_{HF} is stepped through f_{dbl}. Further, we propose that the physics described by (Mjølhus & Flå, 1984) concerning access to the plasma

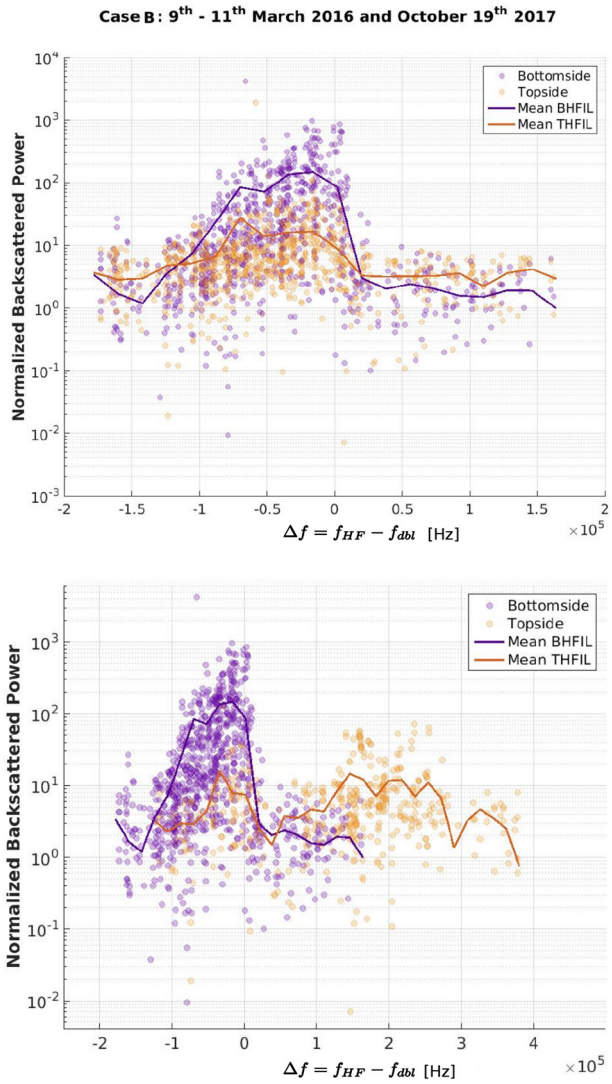

Figure 5. Same as Figure 2 but for the 4 case B high frequency (HF) pulses from October 19th, 2017 and 33 HF pulses with topside high frequency enhanced ion lines, previously presented by Rexer et al. (2018), and all categorized as case B.

resonance through radio windows in a horizontally stratified ionosphere is qualitatively applicable also to artificial radio windows due to the presence of density ducts.

5. Discussion

Figure 2 shows that case A THFIL predominantly appear when f_{HF} is just below or at f_{dbl} at the topside ionosphere, when $\Delta f = f_{\mathrm{HF}} - f_{dbl}$ on the topside is between −100 and 18 kHz. This resembles the dependence of the appearance of THFIL, on the proximity of f_{HF} to f_{dbl} on the bottomside in case B. Both cases of THFIL appear to be asymmetrically conditioned by the proximity of f_{HF} to a f_{dbl}. Contradictory to case B (and our previous observations (Rexer et al., 2018)), case A THFIL appear to be asymmetrically conditioned by the proximity of f_{HF} to f_{dbl} at the topside rather than the bottomside, as for case B.

Case B THFIL appear only simultaneous to stronger BHFIL and are conditioned by the proximity of f_{HF} to f_{dbl} on the bottomside ionosphere. Both THFIL and BHFIL are observed at the altitude where $f_P \approx f_{\mathrm{HF}}$, whereas the matching height is calculated to be approximately ≈6–7 km below the enhancements on the bottomside during the experiment. As the calculations of the matching height are based on the observations of the natural Langmuir waves in the plasma line spectra with a temporal resolution of 1 min, we interpret the observations of the BHFIL at the apparent resonance height to be an indication that large scale density ducts have formed. That is, the matching height is at a higher altitude within the duct, hence the BHFIL appear to be close to the resonance altitude.

In the bottom panel of Figure 5, showing the THFIL and BHFIL related to f_{dbl} at the top- and bottomside, respectively, we see a small local maximum of the case B THFIL when f_{HF} is close to f_{dbl} on the topside (zero on abscissa). This resembles the observations in case A, where THFIL appear to be conditioned by the proximity of f_{HF} to the topside f_{dbl}. It is possible that a similar relation as for case A exists, however, there are few datapoints in this region. As mentioned above, the lower panels of Figure 3 (case B THFIL in the left column) indicate that the range of frequency steps used did not include f_{HF} well below the topside f_{dbl}. It is apparent in the example in the top left panel of Figure 4, that the altitude difference between the bottomside and topside resonance height is≈50 km for case B from October 19th 2017 (≈70–100 km for the observation presented in Rexer et al. (2018)). This leads to a large difference between the top- and bottomside f_{dbl}, as f_G decreases with altitude. As we do not reach this frequency range below f_{dbl} at the topside ionosphere where one might expect THFIL, for these HF pulses, a definite conclusion about a possible relation to f_{dbl} on the topside, also for case B observations, cannot be drawn from these observations.

Further, distinct ion acoustic peaks are observed when $f_{\mathrm{HF}} < f_{dbl}$ on the bottomside and a sharp, distinct $\omega = 0$ peak, associated with the OTSI (i.e., Fejer, 1979; Kuo et al., 1997; Stubbe et al., 1992), in the BHFIL frequency spectra of case B. An example is shown in the middle panels of Figure 4. BHFIL frequency spectra from case A, shown in Figure 1, and BHFIL frequency spectra (not shown) from the downstepping HF pulses on the October 19th, 2017 (right column of Figure 3) have distinct ion acoustic shoulders, associated with PDIs, but only a weak or no $\omega = 0$ feature. Interestingly, although polarization and ERP of EISCAT Heating were the same for all HF pulses on October 19th, 2017, and the frequency steps were spanning the same frequency range, only alternating between stepping upward and downward, the BHFIL spectra for up stepping pulses show a clear and distinct central feature while BHFIL spectra for downstepping pulses show only well developed ion acoustic shoulders and no central feature. The threshold electric field of the

Table 1
Main Characteristics of BHFIL and THFIL for Case A and Case B

	BHFIL	THFIL
Case A		
Observed during f_{HF} downstepping experiments	• Predominantly appear for f_{HF} = 0–100 kHz below the bottomside f_{dbl} • Fade completely for $\Delta f < \sim -100$ kHz • Enhancement at altitude between matching height and resonance height • Weak and fading central feature in ion line spectra	• Predominantly appear when f_{HF} is between ≈ −100 and 18 kHz around the topside f_{dbl} • Growing enhancements as BHFIL fade • Enhancement at resonance height • Filled in ion line spectra/weak central feature
Case B		
Observed during f_{HF} upstepping experiments	• Strong enhancements when f_{HF} is 80 kHz below, and ∼9.8 kHz above the bottomside f_{dbl} • BHFIL abruptly disappear as f_{HF} increases above the bottomside f_{dbl} • Stronger than THFIL • Enhancement appears to be at the resonance height • Prominent, distinct central feature in ion line spectra	• Only appear simultaneous to BHFIL, when f_{HF} is 80 kHz below, and ∼9.8 kHz above f_{dbl} at the bottomside • Weaker then BHFIL • Enhancement at resonance height • Filled in ion line spectra/weak central feature

Abbreviations: BHFIL, bottomside HF-enhanced ion lines; HF, high frequency; THFIL, topside HF-enhanced ion lines

pump wave required to excite the OTSI is usually higher than that for the PDI (Robinson, 1989), indicating a possible difference in allocation of pump wave energy, a difference in *D*-region absorption or different mechanisms responsible for the BHFIL in the up stepping and down stepping HF pulses. The down stepping HF pulses on 19th October are comparable to HF pulses on 18th October, where case A THFIL were observed. We consider it likely that case A THFIL could have been generated also on the downstepping HF pulses on 19th October, had the f_{HF} stepping scheme extended to frequencies below f_{dbl} on the topside ionosphere as discussed above.

In case A, for the duration of the THFIL, f_{HF} is well below f_{dbl} at the bottomside. Consequently anomalous absorption is effective and less energy available for excitation of Langmuir waves and related nonlinear wave interactions at the bottomside plasma resonance (Stubbe et al., 1994). Conforming to this is the absence or very weak BHFIL observed during case A. The proximity of the f_{HF} to f_{dbl} at the topside, by propagation of the pump wave through an artificial radio window, allows for direct linear conversion of the pump wave here (Mjølhus & Flå, 1984). Furthermore, Mjølhus and Flå (1984) predict the formation of strongly nonlinear Langmuir wave field as a result of linear conversion in the resonance region. At exactly the radio window complete transmission occurs, while partial transmission and partial reflection occur for rays near this. It is possible then, that the close proximity of f_{HF} to the topside resonance allows for THFIL also in a suppressed pump field due to the anomalous absorption in the bottomside.

In case B f_{HF} is below f_{dbl} on the bottomside ionosphere for approximately 1 min and the duration of several frequency steps, permitting the development of large scale density ducts (Basu et al., 1997). The Weak BHFIL observed during this time are consistent with this, as the wave energy is absorbed by upper hybrid phenomena a few kilometer below the matching height and associated anomalous absorption (Robinson, 1989). Although we do not have direct observations of density ducts, we argue that it is likely they were excited by the pump wave. The large electron temperature enhancements we observe (up to ∼3500 K), during HF pulses are significantly larger than what is obtained with Ohmic heating alone (Bryers et al., 2013). Such anomalous heating is attributed to resonant heating effects at the upper hybrid resonance altitude, that are strongly coupled to the generation of field aligned density striations (A. V. Gurevich, 2007; A. V. Gurevich et al., 1996; Istomin & Leyser, 1997).

As f_{HF} approaches f_{dbl} on the bottomside, the growth of the density striations is suppressed (Honary et al., 1999; Huang & Kuo, 1994; Mjølhus, 1993; Robinson, 1989) and pump wave energy is guided by the remaining ducts to reach the resonance altitude, permitting coupling to Langmuir and ion acoustic waves.

This can be seen as an increase in the BHFIL power, observed near the resonance altitude, as f_{HF} approaches f_{dbl}. Hence, a larger portion of the pump wave energy reaches the topside resonance region, compared to case A, by propagation in the *L* mode guided by large scale density ducts. THFIL are therefore observed as a result of partial reflection of *Z* mode rays just outside the central ray in the density duct.

With the above discussion in mind the main difference between case A and case B appears to be the allocation of pump wave energy for the generation of BHFIL and the relative proximity of f_{HF} to a f_{dbl}, either on the topside or on the bottomside.

6. Conclusions

We have shown two cases, with different characteristics, of systematically recurring THFIL during an experiment at the EISCAT Heating facility on October 18th and 19th, 2017. A pump wave with an O mode polarization was transmitted in the magnetic zenith direction in a 2-min-on, 5-min-30-sec-off cycle, stepping through the double resonance frequency of the electron gyro frequency and the local upper hybrid frequency. Plasma parameters were obtained from the EISCAT UHF radar, allowing for high accuracy calculations of the altitude profile of the plasma-, upper hybrid-, and *L* mode cut-off frequencies. In case A, THFIL were observed when f_{HF} is at or below the double resonance frequency at the topside ionosphere. No or weak BHFIL were observed at the pump frequencies of the strongest THFIL. In case B observations the THFIL occur simultaneous to BHFIL, when f_{HF} is at or below the bottomside double resonance frequency. These are consistent with previous observations of THFIL made by Rexer et al. (2018) and Borisova et al. (2020). We interpret the observations as a result of pump wave guiding into the *L* mode by large scale density ducts to propagate through the ionospheric density peak. The pump wave may access the plasma resonance through these artificial radio windows in the magnetic zenith direction, in the same manner as Mjølhus and Flå (1984) describe theoretically for natural radio windows in a horizontally stratified ionosphere. We suggest that the main difference between the two characteristic cases of THFIL is the amount of available pump wave energy that reaches the topside resonance region and the relative proximity of the pump wave frequency to the double resonance frequency at the topside resonance region for case A and the bottomside resonance region for case B.

Data Availability Statement

The data of EISCAT UHF radar during the experiment can be obtained from EISCAT https://portal.eiscat.se/schedule/. The EISCAT ISR analysis tool GUISDAP is available at https://eiscat.se/scientist/user-documentation/guisdap/.

Acknowledgments
EISCAT is an international association supported by research organizations in China (CRIRP), Finland (SA), Japan (NIPR and ISEE), Norway (NFR), Sweden (VR), and the United Kingdom (UKRI).

References

Basu, S., Costa, E., Livingston, R. C., Groves, K. M., Carlson, H. C., Chaturvedi, P. K., & Stubbe, P. (1997). Evolution of subkilometer scale ionospheric irregularities generated by high-power HF waves. *Journal of Geophysical Research*, *102*(A4), 7469–7475. https://doi.org/10.1029/96JA03340

Borisova, T. D., Blagoveshchenskaya, N. F., Kalishin, A. S., Häggström, M. I., & Rietveld, M. T. (2020). Excitation of Langmuir and ion–acoustic turbulence in the high-latitude ionosphere by a high-power HF radio wave simultaneously below and above the F 2-layer maximum. *Radiophysics and Quantum Electronics*, *62*(12), 793–806. https://doi.org/10.1007/s11141-020-10025-z

Bryers, C. J., Kosch, M. J., Senior, A., Rietveld, M. T., & Singer, W. (2013). A comparison between resonant and nonresonant heating at EISCAT. *Journal of Geophysical Research: Space Physics*, *118*(10), 6766–6776. https://doi.org/10.1002/jgra.50605

Budden, K. G. (1980). The theory of radio windows in the ionosphere and magnetosphere. *Journal of Atmospheric and Terrestrial Physics*, *42*(3), 287–298. https://doi.org/10.1016/0021-9169(80)90036-7

Chen, F. (1983). *Introduction to plasma physics and controlled fusion* (2nd ed.). Springer.

Eliasson, B. (2008). Full-scale simulation study of the generation of topside ionospheric turbulence using a generalized Zakharov model. *Geophysical Research Letters*, *35*(11), 1–5. https://doi.org/10.1029/2008GL033866

Eliasson, B., & Leyser, T. B. (2015). Numerical study of upper hybrid to Z-mode leakage during electromagnetic pumping of groups of striations in the ionosphere. *Annales Geophysicae*, *33*(8), 1019–1030. https://doi.org/10.5194/angeo-33-1019-2015

Ellis, G. R. (1956). The Z propagation hole in the ionosphere. *Journal of Atmospheric and Terrestrial Physics*, *8*, 43–54. https://doi.org/10.1016/0021-9169(56)90090-3

Fejer, J. A. (1979). Ionospheric modification and parametric instabilities. *Reviews of Geophysics*, *17*(1), 135–153. https://doi.org/10.1029/RG017i001p00135

Ganguly, S., & Gordon, W. E. (1983). Heater enhanced topside plasma line. *Geophysical Research Letters*, *10*(10), 977–978. https://doi.org/10.1029/gl010i010p00977

Gurevich, A., Hagfors, T., Carlson, H., Karashtin, A., & Zybin, K. (1998). Self-oscillations and bunching of striations in ionospheric modifications. *Physics Letters, Section A: General, Atomic and Solid State Physics*, *239*(6), 385–392. https://doi.org/10.1016/S0375-9601(98)00006-1

Gurevich, A. V. (2007). Nonlinear effects in the ionosphere. *Uspekhi Fizicheskih Nauk, Russian Academy of Sciences*, *177*(11), 1145–1177. https://doi.org/10.3367/UFNr.0177.200711a.1145

Gurevich, A. V., Lukyanov, A. V., & Zybin, K. P. (1996). Anomalous absorption of powerful radio waves on the striations developed during ionospheric modification. *Physics Letters, Section A: General, Atomic and Solid State Physics*, *211*(6), 363–372. https://doi.org/10.1016/0375-9601(95)00970-1

Gurevich, A. V., Zybin, K. P., & Lukyanov, A. V. (1995). Stationary striations developed in the ionospheric modification. *Physical Review Letters*, *75*(13), 2622–2625. https://doi.org/10.1103/physrevlett.75.2622

Hagfors, T., & Lehtinen, M. (1981). Electron temperature derived from incoherent scatter radar observations of the plasma line frequency. *Journal of Geophysical Research*, *86*(A1), 119. https://doi.org/10.1029/ja086ia01p00119

Honary, F., Robinson, T., Wright, D., Stocker, A., Rietveld, M., & McCrea, I. (1999). First direct observations of the reduced striations at pump frequencies close to the electron gyroharmonics. *Annales Geophysicae*, *17*, 1235–1238. https://doi.org/10.1007/s00585-999-1235-6. Retrieved from http://hdl.handle.net/2381/12174

Huang, J., & Kuo, S. P. (1994). A theoretical model for the broad upshifted maximum in the stimulated electromagnetic emission spectrum. *Journal of Geophysical Research*, *99*(A10), 19569–19576. https://doi.org/10.1029/94ja01261

Isham, B., Hagfors, T., Mishin, E., Rietveld, M. T., La Hoz, C., Kofman, W., & Leyser, T. B. (1999). A search for the location of the HF excitation of enhanced ion acoustic and Langmuir waves with EISCAT and the Tromso Heater. *Radiophysics and Quantum Electronics*, *42*(7), 533–543. https://doi.org/10.1007/bf02677559

Isham, B., Kofman, W., Hagfors, T., Nordling, J., Thidé, B., LaHoz, C., & Stubbe, P. (1990). New phenomena observed by EISCAT during an RF ionospheric modification experiment. *Radio Science*, *25*(3), 251–262. https://doi.org/10.1029/RS025i003p00251

Isham, B., Rietveld, M., Hagfors, T., La Hoz, C., Mishin, E., Kofman, W., et al. (1999). Aspect angle dependence of HF enhanced incoherent backscatter. *Advances in Space Research*, *24*(8), 1003–1006. https://doi.org/10.1016/s0273-1177(99)00555-4. Retrieved from http://linkinghub.elsevier.com/retrieve/pii/S0273117799005554

Istomin, Y. N., & Leyser, T. B. (1997). Small-scale magnetic field-aligned density irregularities excited by a powerful electromagnetic wave. *Physics of Plasmas*, *4*(3), 817. https://doi.org/10.1063/1.872175. Retrieved from http://scitation.aip.org/content/aip/journal/pop/4/3/10.1063/1.872175

Istomin, Y. N., & Leyser, T. B. (2001). Diffraction of electromagnetic waves by small scale geomagnetic field-aligned density striations. *Physics of Plasmas*, *8*(10), 4577–4584. https://doi.org/10.1063/1.1399325

Kelley, M. C., Arce, T. L., Salowey, J., Sulzer, M., Armstrong, W. T., Carter, M., & Duncan, L. (1995). Density depletions at the 10-m scale induced by the Arecibo heater. *Journal of Geophysical Research*, *100*(A9), 17367–17376. https://doi.org/10.1029/95ja00063

Kosch, M. J., Mjlhus, E., Ashrafi, M., Rietveld, M. T., Yeoman, T., & Nozawa, S. (2011). Angular dependence of pump-induced bottomside and topside ionospheric plasma turbulence at EISCAT. *Journal of Geophysical Research*, *116*(3), 1–9. https://doi.org/10.1029/2010JA016014

Kuo, S. P., Lee, M. C., & Kossey, P. (1997). Excitation of oscillating two stream instability by upper hybrid pump waves in ionospheric heating experiments at Tromso. *Geophysical Research Letters*, *24*(23), 2969–2972. https://doi.org/10.1029/97GL03054

Leyser, T. B., James, H. G., Gustavsson, B., & Rietveld, M. T. (2018). Evidence of L-mode electromagnetic wave pumping of ionospheric plasma in geomagnetic Zenith. *Annales Geophysicae*, *36*, 900167. https://doi.org/10.1029/2009GL041438

Leyser, T. B., & Nordblad, E. (2009). Self-focused radio frequency L wave pumping of localized upper hybrid oscillations in high-latitude ionospheric plasma. *Geophysical Research Letters*, *36*(24), 1–4. https://doi.org/10.1029/2009GL041438

Mishin, E., Hagfors, T., & Isham, B. (2001). A generation mechanism for topside enhanced incoherent backscatter during high frequency modification experiments in. *Tromsø Geophysical Research Letters*, *28*(3), 479–482. https://doi.org/10.1029/2000GL000122

Mjølhus, E. (1990). On linear conversion in a magnetized plasma. *Radio Science*, *25*(6), 1321–1339.

Mjølhus, E. (1993). On the small scale striation effect in ionospheric radio modification experiments near harmonics of the electron gyro frequency. *Journal of Atmospheric and Terrestrial Physics*, *55*(6), 907–918. https://doi.org/10.1016/0021-9169(93)90030-3

Mjølhus, E., & Flå, T. (1984). Direct access to plasma resonance in ionospheric radio experiments. *Journal of Geophysical Research*, *89*(A6), 3921–3928. https://doi.org/10.1029/JA089iA06p03921

Nordblad, E., & Leyser, T. B. (2010). Ray tracing analysis of L mode pumping of the ionosphere, with implications for the magnetic zenith effect. *Annales Geophysicae*, *28*(9), 1749–1759. https://doi.org/10.5194/angeo-28-1749-2010

Rexer, T., Gustavsson, B., Leyser, T., Rietveld, M., Yeoman, T., & Grydeland, T. (2018). First observations of recurring HF-enhanced topside ion line spectra near the fourth Gyroharmonic. *Journal of Geophysical Research*, *123*, 1–15. https://doi.org/10.1029/2018JA025822

Rietveld, M. T., Isham, B., Grydeland, T., La Hoz, C., Leyser, T. B., Honary, F., et al. (2002). HF-pump-induced parametric instabilities in the auroral E-region. *Advances in Space Research*, *29*(9), 1363–1368. https://doi.org/10.1016/S0273-1177(02)00186-2

Rietveld, M. T., Isham, B., Kohl, H., La Hoz, C., & Hagfors, T. (2000). Measurements of HF-enhanced plasma and ion lines at EISCAT with high-altitude resolution. *Journal of Geophysical Research*, *105*(A4), 7429–7439. https://doi.org/10.1029/1999JA90047610.1029/1999JA900476

Rietveld, M. T., Senior, A., Markkanen, J., & Westman, A. (2016). New capabilities of the upgraded EISCAT high-power HF facility. *Radio Science*, *51*(9), 1533–1546. https://doi.org/10.1002/2016RS006093

Robinson, T. R. (1989). The heating of the high latitude ionosphere by high power radio waves. *Physics Reports*, *179*(2–3), 79–209. https://doi.org/10.1016/0370-1573(89)90005-7

Robinson, T. R., Honary, F., Stocker, A. J., Jones, T. B., & Stubbe, P. (1996). First EISCAT observations of the modification of F-region electron temperatures during RF heating at harmonics of the electron gyro frequency. *Journal of Atmospheric and Terrestrial Physics*, *58*(1–4), 385–395. https://doi.org/10.1016/0021-9169(95)00043-7

Stubbe, P. (1996). Review of ionospheric modification experiments at Troms˜. *Journal of Atmospheric and Terrestrial Physics*, *58*(1–4), 349–368. https://doi.org/10.1016/0021-9169(95)00041-0

Stubbe, P., Kohl, H., & Rietveld, M. T. (1992). Langmuir turbulence and ionospheric modification. *Journal of Geophysical Research*, *97*(A5), 6285–6297. https://doi.org/10.1029/91ja03047

Stubbe, P., Stocker, A. J., Honary, F., Robinson, T. R., & Jones, T. B. (1994). Stimulated electromagnetic emissions an anomalous HF wave absorption near electron gyroharmonics. *Journal of Geophysical Research*, *99*(A4), 6233–6246. https://doi.org/10.1029/94ja00023

Tjulin, A. (2017). EISCAT Experiments. *EISCAT Scientific Association*(March). Retrieved from https://www.eiscat.se/wp-content/uploads/2017/04/Experiments.pdf